JOURNAL OF APPLIED ELECTROCHEMISTRY 19 (1989) 649–656

Role of gas bubbles adsorbed on a carbon electrode: electroreduction of chlorine gas in fused salts*

F. LANTELME, H. ALEXOPOULOS

Laboratoire d'Electrochimie, U.A. 430 C.N.R.S., Université Pierre et Marie Curie, Bt. F, 4 place Jussieu, 75252 Paris Cedex 05, France

O. HAAS

Paul Scherrer Institute (P.S.I.), Villingen-P.S.I., CH-5232 Switzerland

Received 1 September 1988

The reaction $Cl_2 + 2e \Leftrightarrow 2Cl^-$ has been studied by transient electrochemical techniques on a vitreous carbon electrode in fused alkali chlorides. Two regimes have been detected: for small overpotentials the electrode response obeys the classical laws of linear diffusion, for larger overpotentials the electrode behaviour involves the gas coming from the bubbles. A model is presented to describe these mechanisms. Four steps are considered: dissolution of chlorine around a gas bubble, diffusion in the electrolyte, charge transfer and chloride ion migration. The first step is always rapid. The influence of the three other steps is examined. It is indicated that the largest part of the reaction occurs near the triple contact interface. At the very extremity of the tip, charge transfer is the primary limiting factor; it is considered that over a distance of a few atomic diameters the mass transport is very rapid. At the largest distances the diffusion of dissolved chlorine constitutes the main limiting factor. The ohmic drop due to the electrical resistance of the electrolyte remains small. The influence of the interfacial tension and of the shape of the bubbles are predicted. The non-stationary situation is also examined in order to take into account the size variation of the gas bubbles during transient conditions.

1. Introduction

Many electrochemical reactions involve a gaseous component and a great deal of research has been devoted to the study of the specific features of these reactions. Three main areas have been investigated: the bubble formation in electrochemical systems [1], the mass transfer and hydrodynamic instabilities at gas-evolving surfaces [2], and the behaviour of gas electrodes in fuel cells [3]. In this last field the behaviour of porous electrodes [4] and the catalytic properties of the electrode material [5] were studied. However a few works deal with contributions of gas bubbles adsorbed at the electrode surface [6].

The aim of the present paper is to examine this contribution, which may be useful in understanding the behaviour of a gas-fed electrode. We are interested by the chlorine electrode; chlorine gas has been considered as a possible oxidizing reagent for fuel cells using fused salts [7]. Here the chlorine reduction will be studied on a vitreous carbon electrode in a fused eutectic mixture LiCl–KCl with eventual additions of $AlCl_3$, the Al/Cl_2 couple being a possible candidate for energy storage [8]. The electrochemical transient techniques will be used to determine the mechanisms of this reaction. Special attention will be paid to the role of the transport process of the electroactive gas coming from the bubbles and from the bulk of the solution.

2. Experimental details

The LiCl–KCl eutectic mixture was purified by a high vacuum dessication procedure, chlorine bubbling, argon flushing, electrolysis and filtering [9]. The introduction of aluminium chloride was carried out by anodic dissolution of a rod of pure aluminium, the cathode being the chlorine electrode. The electrochemical experiments were carried out under argon at about 450° C. The electrochemical cell consisted of an outer Pyrex envelope at the bottom of which rested the vessel containing the molten bath. In order to observe the formation of gas bubbles a transparent electrical furnace was used. For more details concerning the cell, the electrolyte preparation and the atmosphere purification see [10].

The counter electrode and the reference electrode were chlorine electrodes similar to those described by Chemla and Périé [11]. The working electrodes were rods of vitreous carbon V25 (dia. 3 mm) supplied by Le Carbone Lorraine. For the generation of different potential or current programs a Tacussel PRT 20/10 potentiostat and a Tacussel GSTP4

* Paper presented at the 2nd International Symposium on Electrolytic Bubbles organized jointly by the Electrochemical Technology Group of the Society of Chemical Industry and the Electrochemistry Group of the Royal Society of Chemistry and held at Imperial College, London, 31st May and 1st June 1988.

0021-891X/89 $03.00 + .12

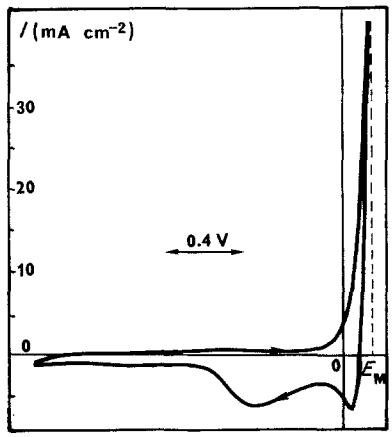

Fig. 1. Voltammogram for the reaction $Cl_2 + 2e \Leftrightarrow 2Cl^-$. Working electrode: vitreous carbon; temperature: 425° C; electrolyte: LiCl–KCl + 1 mol % $AlCl_3$; sweep rate, $v = 0.87\,V\,s^{-1}$; potential of the positive limit of the potential window, $E_M = 0.15\,V$ vs Cl_2/Cl^-.

programmer were used. The transient responses were collected on a Sefram *X/Y* recorder, unless stored in a digital oscilloscope Nicolet 3091 as an intermediate stage.

3. Results

3.1. *Cyclic voltammetry*

Typical voltammograms corresponding to the redox reaction

$$Cl_2 + 2e \Leftrightarrow 2Cl^- \qquad (1)$$

are reported in Figs 1 and 2. The potential is referred to the chlorine electrode. A remarkable increase of the current is observed as soon as positive potentials are reached. This part corresponds to the formation of dissolved chlorine and to the appearance of gas bubbles at the electrode surface; these bubbles grow bigger rapidly; when the potential is positive enough they coalesce. Their shape depends on the bath composition: when the electrolyte does not contain aluminium chloride hemispherical bubbles are observed; their diameter may reach 1 mm and they separate from the electrode with difficulty. On the other hand when aluminium chloride is present (about 1 mol %) the bubbles are spherical and their size is smaller; they easily leave the electrode surface.

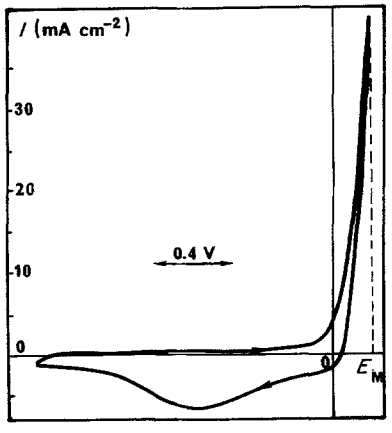

Fig. 2. Voltammogram for the reaction $Cl_2 + 2e \Leftrightarrow 2Cl^-$. Working electrode: vitreous carbon; temperature: 425° C; electrolyte: LiCl–KCl; sweep rate, $v = 5.6\,V\,s^{-1}$; potential of the positive limit of the potential window, $E_M = 0.2\,V$ vs Cl_2/Cl^-.

The backward voltammograms are characterized by one or two maxima. In a general way the appearance of two maxima depends on the value, E_M, of the positive side of the potential window. For not too positive values of E_M and for not too slow sweep rate, only one reduction peak is observed in the vicinity of the potential of the reference electrode, mainly when aluminium chloride is present in the electrolyte. The second reduction peak appears when E_M is positive enough to induce the formation of gas bubbles at the electrode surface. For a given potential window the peak height increases when the potential sweep rate becomes slower, which makes the peak separation clearer. Finally for higher E_M ($E_M > 0.15\,V$) the second peak overlaps the first one and only one peak is observed, particularly when a pure LiCl–KCl electrolyte is used.

3.2. *Current step*

When suitable conditions are chosen two potential plateaux can be observed during the passage of a reduction current of constant intensity (Fig. 3). The durations of the two plateaux differ by several orders of magnitude: a few milliseconds for the first one, τ_1, about one second for the second one, τ_2. As for the cyclic voltammetry the most negative plateau exists only when gas bubbles are present on the electrode surface, i.e. when the starting potential is sufficiently positive. The separation between the two plateaux is made more visible when higher current densities are used.

4. Discussion

The Cl_2 overall reduction process in alkali chloride melt can be separated into four steps: dissolution of chlorine in the melt, diffusion of chlorine to the carbon–electrolyte interface, electron transfer and migration of chloride ions. The first step is rapid compared to the others; the third step has an exchange current density of about $0.06\,A\,cm^{-2}$, which means that at a current density of about $0.1\,A\,cm^{-2}$ the activated polarization is about 0.09 V. The second and third steps remain the main rate-determining steps.

The existence of two reduction peaks in cyclic voltammetry or of two plateaux in chronopotentiometry indicates that two mechanisms can be considered, one of them (occurring at the most negative potentials) being clearly linked to the presence of gas bubbles. In order to analyse these two mechanisms we start this study by examining the results of transient techniques performed in the vicinity of the zero potential; indeed in this region only one mechanism seems to be involved.

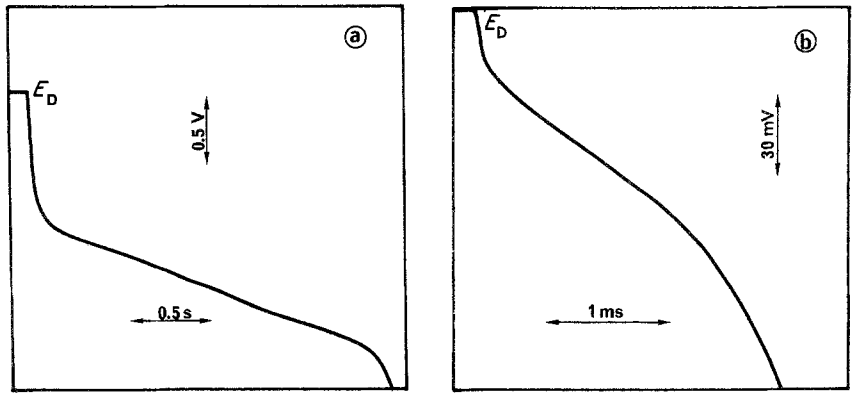

Fig. 3. Chronopotentiogram for the reduction of Cl_2. Working electrode: vitreous carbon; temperature: 425° C; electrolyte: LiCl–KCl; starting potential, E_D = 0.05 V vs Cl_2/Cl^-; current density, 0.035 A cm^{-2}. (a) Long time scale; (b) short time scale.

4.1. *Analysis of the voltammograms; small potential window*

Typical voltammograms carried out in the region of the zero potential are reported in Fig. 4. Their shape is in good agreement with a diffusion-controlled reaction when the reactant concentration remains constant. The theoretical analysis of these voltammograms was carried out recently [12]. Using this analysis theoretical voltammograms can be calculated when the diffusion coefficient, D_{Cl_2}, and the concentration, $C^0_{Cl_2}$, of the dissolved chlorine in equilibrium with the chlorine gas at one atmosphere are known. To perform these calculations the value, D_{Cl_2}, is deduced from the equation in Table 2. By a trial and error process the values of $C^0_{Cl_2}$ are calculated in order to fit the theoretical curves with the experimental ones. These values are in agreement with the result of chemical determinations, which gives $C^0_{Cl_2} = 1.39 \times 10^{-7}$ mol cm^{-3} at 450° C [14]. The reaction 1 being rapid and the current densities not too large, the surface concentration of dissolved chlorine obeys the Nernst equation

$$C_{Cl_2} = C^0_{Cl_2} \exp [nF(E - E^0)/RT] \qquad (2)$$

E^0 is the standard potential of reaction 1.

4.2. *Analysis of the first wave of the chronopotentiograms*

This analysis confirms the preceding mechanism, i.e. the role of the diffusion of dissolved chlorine molecules; as shown in Fig. 5 the plot of the function $E(t)$ vs ln $[(t^{1/2} - \tau^{1/2})/\tau^{1/2}]$ exhibits a large linear part [15] and the slope of this straight line gives the electron number, $n \simeq 2$ (Table 1). Moreover from the values of the transition times, τ, and from the previous value of the diffusion coefficient, D_{Cl_2}, the value of the chlorine concentration at the beginning of the pulse can be calculated according to Sand's law [16]. As shown in Table 1 these values are similar to those deduced from the starting potential, E_D, using the Nernst law (2) and the value, $C^0_{Cl_2}$, deduced from Table 2. The gap between these two values remains within the range of accuracy of the experimental determinations. However the systematic deviation ($C^*_{Cl_2 Sand} > C^*_{Cl_2 Nernst}$) may be an indication of the formation of a carbon–chlorine compound at the electrode surface; the presence of such compounds has been considered to explain the behaviour of graphite electrodes [6].

The behaviour of the chlorine electrode in the vicinity of the zero potential is controlled by the

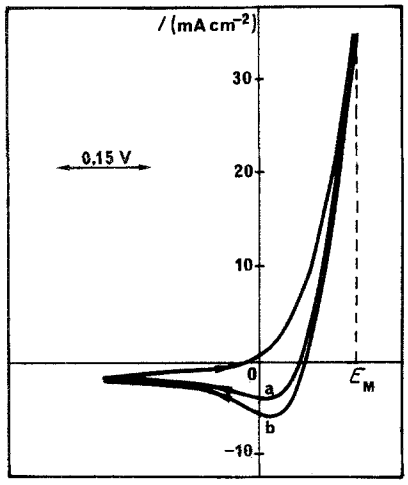

Fig. 4. Voltammograms for the reaction $Cl_2 + 2e \Leftrightarrow 2Cl^-$. Working electrode: vitreous carbon; temperature: 425° C; electrolyte: LiCl–KCl + 1 mol % $AlCl_3$; sweep rate: (a) $v = 2.5$ V s^{-1}; (b) $v = 5.0$ V s^{-1}; potential of the positive limit of the potential window, E_M = 0.15 V vs Cl_2/Cl^-; potential window 0.42 V.

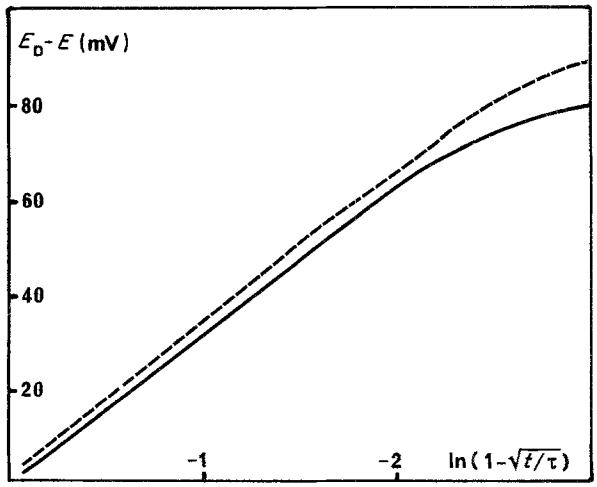

Fig. 5. Plots E_D–E vs ln $(1 - t^{1/2}/\tau^{1/2})$ in the short time region of the chronopotentiograms. Continuous line: chronopotentiogram reported in Fig. 3. Pecked line: working electrode: vitreous carbon; starting potential, E_D = 0.05 V vs Cl_2/Cl^- electrode; electrolyte: LiCl–KCl + 1 mol % $AlCl_3$; i = 8 mA cm^{-2}; τ_1 = 7.5 ms.

Table 1. Results deduced from the first wave of the chronopotentiograms (see for example Fig. 3b). Working electrode: vitreous carbon; E_D: starting potential; i: current density; τ_I: transition time; n: number of electrons; $C^*_{Cl_2}$: concentration of dissolved chlorine. Values deduced from the theory of linear diffusion (Sand's law) and from the Nernst's law at the starting potential E_D

	E_D (mV vs Cl_2/Cl^-)	i ($mA\,cm^{-2}$)	τ_I (ms)	n	$C^*_{Cl_2}$ (Sand) (10^{-6} mol cm^{-3})	$C^*_{Cl_2}$ (Nernst) (10^{-6} mol cm^{-3})
	50	35	1.7	1.95	2.78	0.72
Electrolyte:	20	5	20	1.9	1.31	0.27
LiCl–KCl	0	2	25	2.1	0.60	0.14
Temperature:	0	3	11.5	1.5	0.62	0.14
698 K	0	4	7.3	1.9	0.63	0.14
	0	5	4.2	1.8	0.62	0.14
Electrolyte:	40	16	1.8	1.95	1.08	0.57
LiCl–KCl +	40	8	7.5	1.8	1.10	0.57
1 mol % $AlCl_3$	40	4	24	1.7	1.00	0.57
Temperature:	40	2	216	1.8	1.49	0.57
743 K						

diffusion of dissolved chlorine. Some departure from the classical law of diffusion-controlled reaction appears when the potential of the electrode becomes sufficiently positive, i.e. when gas bubbles appear at the electrode surface. As pointed out above these bubbles are involved in the electrochemical process which gives rise to the second peak observed in the cyclic voltammetry or to the second plateau observed in the chronopotentiometry.

4.3. *Role of the gas bubbles in chlorine reduction*

It is considered that when a bubble is present at the electrode surface the electrochemical reaction is driven by the reduction of the dissolved chlorine coming from the bubble. This process is illustrated by the diagram in Fig. 6. The contact angle, θ, depends on the interfacial properties of the system. At the electrode surface the current dI which flows through an annulus of thickness, dr, and radius $r_0 + r$, is given by

$$dI = -2\pi(r_0 + r)nFD_{Cl_2}(\partial C_{Cl_2}/\partial y)_{y=0}\,dr \quad (3)$$

As the main part of the current comes from the region near the triple contact (small r) the concentration gradient is written

$$(\partial C_{Cl_2}/\partial y)_{y=0} = (C_s - C_r)/\delta \quad (4)$$

C_s and C_r are the concentrations of the dissolved chlorine near the gas bubble and at the electrode surface; it is supposed that the chlorine follows the path, $\overset{\frown}{PM}$, whose length, δ, is

$$\delta = r\theta' \quad (5)$$

with

$$\theta' = \theta + \theta_1$$

and

$$\theta_1 = \arcsin(r \sin\theta/2r_0) \quad (6)$$

The chlorine dissolution being rapid, the concentation, C_s, of dissolved chlorine in the electrolyte in contact with the gas bubble is $C^0_{Cl_2}$ given in Table 2; it is considered that the overpressure due to the curvature of the interface is negligible. The concentration, C_r, in Equation 4 is related to the potential at the point P. This potential depends on the electrode overpotential, η_b (here η_b and I are negative). At the point P this overpotential can be separated into two parts, $\eta_b = \eta_R + \eta_{DT}$, the first term represents the ohmic drop due to the current flowing through the electrolyte, the second the diffusion and charge transfer overpotential.

The elementary resistance of the shell of thickness, dr, generated by the rotation of the arc, $\overset{\frown}{PM}$, around the y axis, $\overrightarrow{BD}$, is

$$dR_e = (\varrho_e/S)\,dr \quad (7)$$

Table 2. Temperature dependence of some physicochemical parameters used in this paper (T in K)

Electrolyte conductance κ ($\Omega^{-1}\,cm^{-1}$) [18]:

$$\kappa = -5.6492 + 1.3732 \times 10^{-2}\,T - 5.1788 \times 10^{-6}\,T^2$$

Chlorine diffusion coefficient D_{Cl_2}($cm^2\,s^{-1}$) [13]:

$$D_{Cl_2} = 3.6 \times 10^{-2} \exp(-4156/T)$$

Chlorine solubility C_{Cl_2} (mol cm^{-3}) at one atmosphere [14]:

$$C^\circ_{Cl_2} = (5.85 \times 10^{-3}(T - 273) - 1.11) \times 10^{-7}$$

Exchange current density i_0($A\,cm^{-2}$) [19]:

$$i_0 = 7.8 \exp(-3442/T)$$

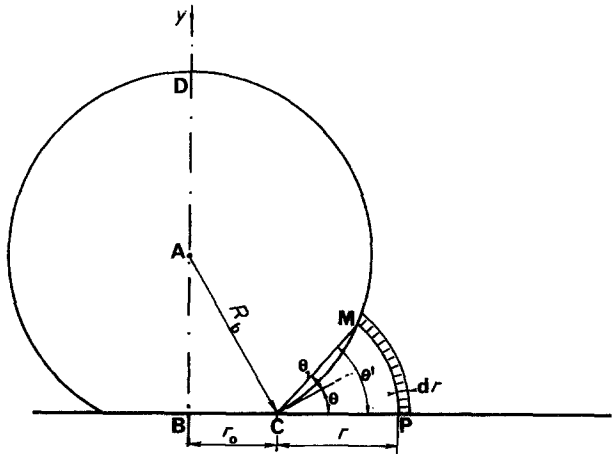

Fig. 6. Geometry of the gas bubble.

ϱ_e being the electrical resistivity of the electrolyte; its surface is

$$S = 2\pi r(r_0\theta' + r \sin \theta') \quad (8)$$

The ohmic drop due to the passage of a current, I, through this shell is

$$d\eta_R = I\, dR_e \quad (9)$$

with

$$I = \int_0^r dI \quad (10)$$

dI being given by Equation 3. For a not too large current density the concentration, C_r, is given by the Nernst equation (Equation 2) where $E = E^0 + \eta_{DT}$. However the current density increases considerably near the tip of the triple contact and the charge transfer kinetics has to be considered; the concentration, C_r, is then deduced from the equation

$$dI = 2\pi(r + r_0)i_0\{\exp[(1 - \alpha)F\eta_{DT}/RT] - (C_r/C_s)\exp(-\alpha F\eta_{DT}/RT)\}\, dr \quad (11)$$

The behaviour of a gas bubble is examined by a finite step technique. A small radius increment, Δr ($\Delta r \simeq 10^{-8}$ cm), is used. The ultimate distance which is reasonable to use near the triple contact point, C, is of the order of two or three atomic diameters, here we consider that the thin liquid layer between the gas and the electrode must have a thickness greater than 10 Å to be taken into account in the calculations; the same limitation was introduced by Bockris and Cahan [16] in their model of finite contact meniscus.

To start the calculation an arbitrary value, η_{DT_1}, of the overpotential, η_{DT}, is chosen for the first element, Δr, near the triple contact. The current, ΔI_1, and the surface concentration, C_{s_1}, are calculated from Equations 3, 4 and 11 with $\alpha = 0.5$. The ohmic drop, $\Delta\eta_{R1}$, in the first shell is deduced from Equation 9. The overpotential in the second shell is $\eta_{DT_2} = \eta_{DT_1} + \Delta\eta_{R_1}$. A recurrent process is started; the overpotential

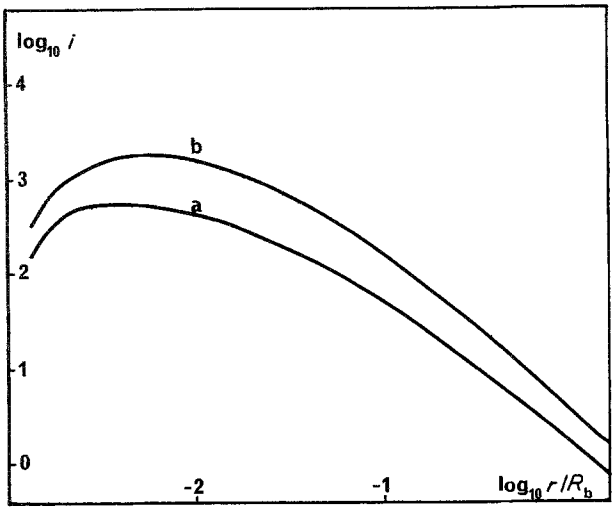

Fig. 7. Calculated local current density around a gas bubble; $R_b = 10\,\mu$m; overpotential $\eta_b = 0.72$ V vs Cl_2/Cl^- electrode; contact angle $\theta = 5°$; temperature 698 K; curve a: model with a constant diffusion coefficient D_{Cl_2}; curve b: model using a variable diffusion coefficient (Equation 14), $\delta_c = 1.7 \times 10^{-6}$ cm.

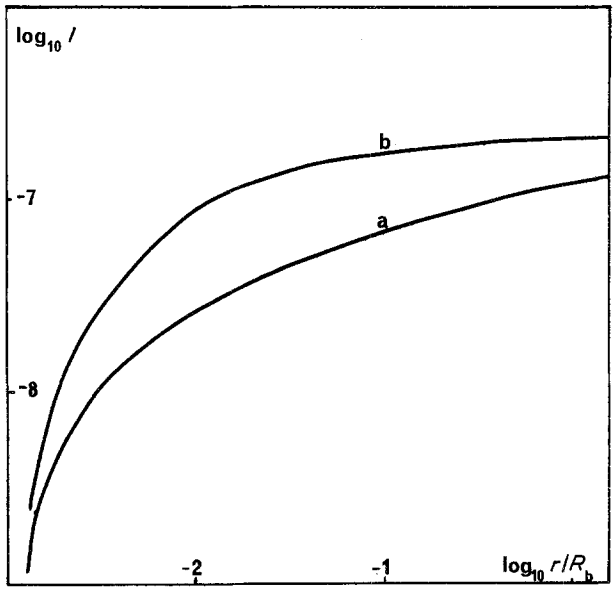

Fig. 8. Calculated current I around a gas bubble, Equation 10; $R_b = 10\,\mu$m; overpotential, $\eta_b = 0.72$ V vs Cl_2/Cl^- electrode; contact angle, $\theta = 5°$; temperature: 698 K; curve a: model with a constant diffusion coefficient D_{Cl_2}; curve b: model using a variable diffusion coefficient (Equation 14), $\delta_c = 1.7 \times 10^{-6}$ cm.

in the jth shell is $\eta_{DT_j} = \eta_{DT_{j-1}} + \Delta\eta_{R_{j-1}}$ and $I_j = I_{j-1} + \Delta I_{j-1}$. For large j values the variations $\Delta\eta_{R_j}$ and ΔI_j become small and larger values of Δr can be used. It is shown that η_{DT_j} and I_j tend rapidly towards limiting values, η_b and I_b, for large j. By a trial and error process η_{DT_1} is varied in order either that η_b fit the experimental overpotential (potentiostatic experiments) or that I_b corresponds to the experimental current (galvanostatic experiments). As an example the current density and the current around a gas bubble are reported in Figs 7 and 8 (curves a).

The computed current density near the tip can be of the order of 100–1000 A cm^{-2}. Accompanying this high current density is a correspondingly high power loss of several W cm^{-2}. However the heat effect remains small. The thermal conductivity of the electrode material is high and its temperature can be considered as constant. Moreover the heat dissipation in this thin region is rapid. The thermal conductivity of the electrolyte is about 66×10^{-4} J cm^{-1} s^{-1} K^{-1} [17]. A simple calculation shows that the temperature increase in this region remains negligible.

The influence of the overpotential, η_b, on the current, I_b, for two contact angles is illustrated in Fig. 9 (pecked line); the current being roughly proportional to the radius, R_b, the quantity I_b/R_b was introduced. These curves show the existence of a limiting current.

The preceding scheme is relative to a stationary state. To interpret the results of transient techniques it is required to take into account the variations of the volume of the gas bubble due to the chlorine consumption. A finite step procedure is used. During a time step, Δt, the volume change, ΔV, is

$$\Delta V = I_b V_m \Delta t/nF \quad (12)$$

V_m being the molar volume of the gas. The new volume, $V_{t+\Delta t} = V_t - \Delta V$, is calculated and the radius

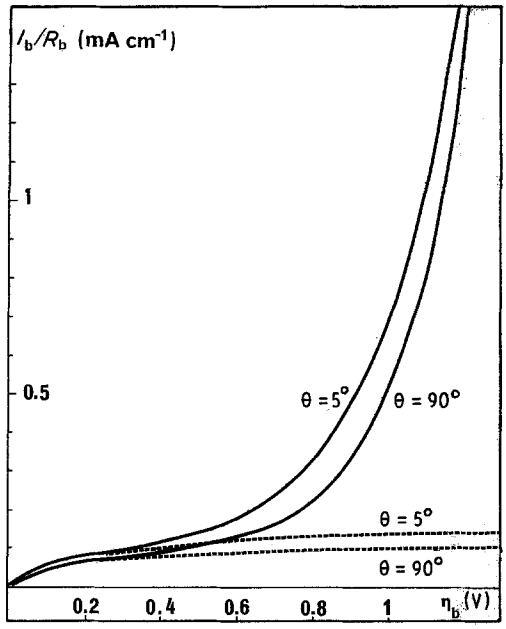

Fig. 9. Variation of the calculated quantity I_b/R_b vs the overpotential η_b, I_b is the current and R_b the radius of the bubble, here $R_b = 10\,\mu m$; temperature: 698 K. (a) Dashed line: model using a constant diffusion coefficient D_{Cl_2}; (b) continuous line: model using a variable D_{Cl_2} at the atomic scale (Equation 14), $\delta_c = 1.7 \times 10^{-6}$ cm.

for the next step becomes

$$R_b = \{3V_{t+\Delta t}/\pi(1 + \cos\theta)^2(2 - \cos\theta)\}^{1/3} \quad (13)$$

To start the calculation it is considered that a certain number, N_b, of bubbles of radius, R_b, exist at the beginning of the experiment (or at the positive extremity of the potential window in cyclic voltammetry). The contribution of the bulk diffusion and that of the gas bubbles are calculated according to the finite step technique.

The different physicochemical parameters (chlorine diffusion coefficient and solubility, electrical resistivity) required by the model are deduced from literature data. An Arrhenius representation is used to describe their temperature dependence (Table 2); an estimate of the exchange current density is also obtained from experiments carried out in pure LiCl. [19]. The contact angle depends on the nature of the electrolyte. The visual observations indicate that $\theta = 90°$ in pure LiCl–KCl. When $AlCl_3$ is introduced θ becomes very small, a value $\theta = 5°$ is chosen for the calculations. The number, N_b, and the radius, R_b, are adjusted in order to fit the experimental curves.

This approach gives a good representation of the experimental curves. However the calculated values found for the bubble characteristics do not fit the experimental observations very well. The mean calculated radius is too small and the number of bubbles is too large. We think that this departure comes from the description of the chlorine flow in the tip of the meniscus; at the very extremity of this triple contact region the transport occurs through a few atomic layers. At this scale the concept of diffusion itself vanishes [20]; in the first atomic layer the only transport limitation is the instantaneous velocity of the particles which is very large. Moreover in this boundary region the structure of the medium can be perturbed; as indicated by Vogt [21] the concentration of dissolved gas can be greater than that existing in the bulk of the liquid and also the contact angle can vary at atomic scale which perturbs the geometry used to describe the region near the triple contact.

Our knowledge of the structure of this region is not yet accurate enough to give a definite description of the phenomenon occurring at the very extremity of the meniscus. To retain the previous scheme it should be considered that at atomic distances the diffusion coefficient tends towards infinity. In the boundary region the flux of active species is more rapid than in the bulk phase. A similar effect has recently been invoked to explain the behaviour of alloy formation in the very first layers of alloy coatings [22]. In agreement with these ideas it is supposed that the diffusion coefficient introduced in Equation 3 varies according to the equation

$$D_{Cl_2} = D^{\infty}_{Cl_2} \exp(\delta_c/\delta) \quad (14)$$

where $D^{\infty}_{Cl_2}$ is the bulk diffusion coefficient and δ_c a characteristic distance. The electrochemical behaviour of a gas bubble is again examined in the framework of the preceding model in which Equation 14 is introduced. The current density and the current around a gas bubble are reported in Figs 7 and 8 (curves b); the total current, I_b, vs the overpotential, n_b, is reported in Fig. 9 (continuous line).

Taking into account this hypothesis leads to a correct interpretation of the experiments. The intro-

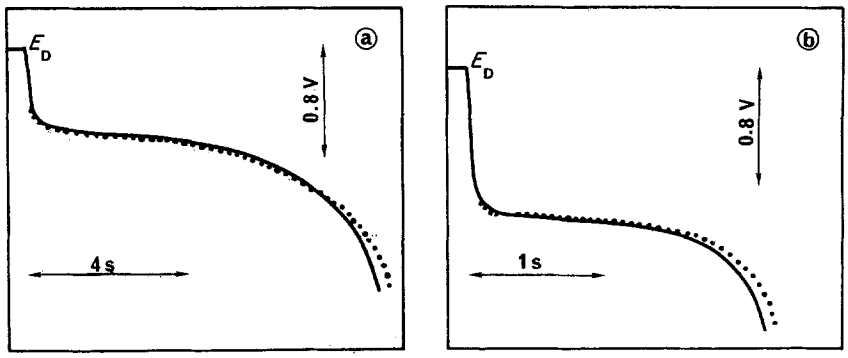

Fig. 10. Experimental (continuous line) and simulated (dotted line) chronopotentiograms. Working electrode: vitreous carbon; temperature: 698 K; starting potential $E_D = 0.05$ V vs Cl_2/Cl^- electrode; electrolyte: LiCl–KCl + 1 mol % $AlCl_3$; (a) current density, $i = 5\,mA\,cm^{-2}$; (b) $i = 15\,mA\,cm^{-2}$.

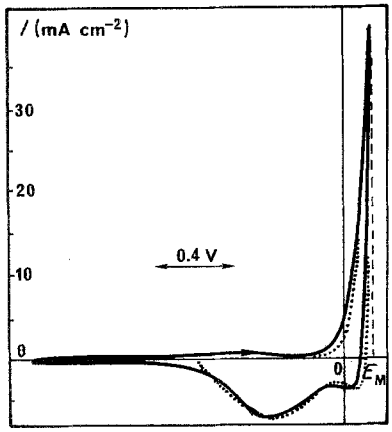

Fig. 11. Experimental (continuous line) and simulated (dotted line) voltammograms. Working electrode: vitreous carbon; temperature: 698 K; electrolyte: LiCl–KCl + 1 mol % $AlCl_3$; sweep rate, $v = 0.425\,V\,s^{-1}$; potential of the positive limit of the potential window, $E_M = 0.15$ V vs Cl_2/Cl^- electrode.

duction of a critical distance, $\delta_c \simeq 170$ Å, gives a suitable representation of the experimental curves: some simulated chronopotentiograms and voltammograms are drawn in Figs 10 and 11. The size and number of gas bubbles (Table 3) deduced from that model are in good agreement with the experimental observations. The influence of the wettability of the electrode material is detected. With a pure LiCl–KCl electrolyte which does not wet the vitreous carbon significantly ($\theta = 90°$) the model predicts the existence of a small number of bubbles (dia. $\simeq$ 0.3 mm). When aluminium chloride is added to the bath the wettability increases and the size of bubbles decreases (dia. $\simeq$ 0.1 mm), whereas their number increases.

5. Conclusions

The reduction of chlorine present in gas bubbles adsorbed at the electrode surface on a vitreous carbon electrode has been studied by transient techniques. It is indicated that initially the reaction is controlled by the linear diffusion of the chlorine dissolved in the bulk of the electrolyte. Rapidly the contribution of the chlorine coming from the bubble becomes predominant. The model proposed to describe this reaction involves four steps. First the dissolution of chlorine into the electrolyte occurs; this process is rapid and the electrolyte layer in contact with the gas is saturated with chlorine. This chlorine diffuses towards the electrode where it is reduced. The created chloride ions migrate towards the bulk of the electrolyte.

Most of the current is produced at the tip of the meniscus; the length of the active zone around the triple contact represents a few per cent of the bubble radius. In this region the diffusion and activation processes control the reaction. Special attention should be paid to the phenomena which occur at the very extremity of the meniscus when the thickness of the electrolyte layer reaches atomic dimensions. As already pointed out the diffusion concept is no longer valid at this very short distance and the main limiting factor is the activation process and the ohmic drop in the electrolyte.

The approach developed indicates the role of some physicochemical parameters such as the electrical resistivity of the electrolyte, the charge transfer kinetics, the gas solubility and the diffusion coefficient of dissolved gas. It is shown that the geometry of the meniscus in the three-phase region influences the behaviour of the electrochemical reaction; it is then possible to take into account the effect of the interfacial properties of the solid–gas–liquid system. This fundamental approach may be useful in determining the choice of materials and the design of porous gas electrodes required for fuel cell technology.

Table 3. Reduction of chlorine gas coming from bubbles adsorbed at the electrode surface. Galvanostatic conditions; working electrode: vitreous carbon; starting potential: $E_D = 0.05$ V vs Cl_2/Cl^- electrodes; temperature: 698 K; i: current density; τ_2: experimental transition time; N_b and R_b, number (cm^{-2}) and radius of the gas bubbles introduced in the calculation to simulate the experimental chronopotentiograms (see Fig. 10)

	i (mA cm^{-2})	τ_2 (s)	N_b	R_b (mm)
Electrolyte:	1.5	50	320	0.31
LiCl–KCl	6	15	280	0.33
	20	5	210	0.37
	35	2.2	330	0.30
Electrolyte:	5	8.9	1680	0.12
LiCl–KCl +	10	3.6	1612	0.124
1 mol % $AlCl_3$	15	1.9	2177	0.096

Acknowledgement

One of the authors (H.A.) is deeply indebted to the Swiss Federal Institute Paul Scherrer for financial support.

References

[1] Yu. G. Chirkov and A. G. Psenichnikov, *Soviet Electrochem.* **21** (1986) 114; Ext. Abstracts, 37th Meeting of the International Society of Electrochemistry, Vilnius, USSR, August (1986) p. 283.
[2] G. Kreysa and M. Kuhn, *J. Appl. Electrochem.* **15** (1985) 517.
[3] S. H. White and U. M. Twardoch, *J. Electrochem. Soc.* **135** (1988) 893.
[4] J. S. Dunning, D. N. Bennion and J. Newman, *J. Electrochem. Soc.* **118** (1971) 1251; see also [16].
[5] J. O'M. Bockris and A. K. N. Reddy, 'Modern Electrochemistry', Plenum, New York (1970) p. 1383.
[6] H. Alexopoulos, Thesis, University Pierre et Marie Curie, Paris, July (1988).
[7] D. A. Swinkels, in 'Advances in Molten Salt Chemistry' (edited by J. Braunstein, G. Mamantov and G. P. Smith), Plenum, New York (1971) Vol. 1, p. 165.
[8] F. Lantelme, H. Alexopoulos, M. Chemla and O. Haas, *Electrochim. Acta* **33** (1988) 761.
[9] T. Vargas and D. Inman, *J. Appl. Electrochem.* **17** (1987) 270.
[10] F. Lantelme, D. Inman and D. G. Lovering, in 'Molten Salt Techniques', Plenum, New York (1984) Vol. 2, p. 137.
[11] M. Chemla and J. Périé, French Patent No. 1332 518 (1963).
[12] F. Lantelme and E. Cherrat, *J. Electroanal. Chem.* **244** (1988) 61.
[13] G. J. Janz, C. B. Allen, N. P. Bansal, R. M. Murphy and R. P. T. Tomkins, 'Physical Properties Data Compilations Relevant to Energy Storage', NSRD–NBS 61,

U.S. Department of Commerce, Washington (1979) Part II, p. 234.
[14] J. D. Van Norman and R. J. Tivers, in 'Molten Salts, Characterization and Analysis' (edited by G. Mamantov), Marcel Dekker, New York (1969); see also T. Nakajima, H. Imoto, K. Nakanishi and N. Watanabe, *Denki Kagaku* **42** (1974) 85.
[15] A. J. Bard and L. R. Faulkner, 'Electrochemical Methods' John Wiley, New York (1980) p. 256.
[16] J. O'M. Bockris and B. D. Cahan, *J. Chem. Phys.* **50** (1969) 1307.
[17] M. V. Smirnov, V. A. Khokhlov and E. S. Filatov, *Electrochim. Acta* **32** (1987) 1019.
[18] Ref. [13], p. 228.
[19] W. E. Triaca, C. Salomons and J. O'M. Bockris, *Electrochim. Acta* **13** (1968) 1942.
[20] F. Lantelme and P. Turq, *J. Chem. Phys.* **81** (1984) 5046.
[21] H. Vogt, *Electrochim. Acta* **29** (1984) 167.
[22] F. Lantelme, A. Derja and N. Kumagai, *J. Electroanal. Chem.* **248** (1988) 369.